

3D Endoscope System Using Asynchronously Blinking Grid Pattern Projection for HDR Image Synthesis

Ryo Furukawa^{1(✉)}, Masahito Naito¹, Daisuke Miyazaki¹, Masahi Baba¹, Shinsaku Hiura¹, Yoji Sanomura², Shinji Tanaka², and Hiroshi Kawasaki³

¹ Hiroshima City University, Hiroshima, Japan
{ryo-f,miyazaki,baba,hiura}@hiroshima-cu.ac.jp,
naito@ime.hiroshima-cu.ac.jp

² Hiroshima University Hospital, Hiroshima, Japan
{sanomura,colon}@hiroshima-cu.ac.jp

³ Kyushu University, Fukuoka, Japan
kawasaki@ait.kyushu-u.ac.jp

Abstract. 3D endoscopic systems have been researched and developed to measure the actual shape and size of living tissues for the purpose of remote surgery and diagnosis, to name a few. For such systems, active stereo that consists of a camera and a pattern projector (*i.e.*, structured light systems) is a promising solution because of simple system with high accuracy. Recently, an active-stereo-based 3D endoscope system has been proposed, in which many practical problems were solved such as shallow focal range of the pattern projector or strong diffusion by living tissues. To use the laser pattern projector for endoscopic systems, two fundamental issues arise; a limited dynamic range of the endoscopic camera and a calibration of the system. In this paper, we proposed a new high dynamic range (HDR) image synthesis technique for a laser pattern projector as well as an auto-calibration technique for dynamic motion. Quantitative experiments are conducted to show the effectiveness of the method followed by a demonstration using real endoscopic system.

1 Introduction

3D endoscopic systems have been intensively researched and developed to measure the actual shape and size of living tissues for the strong demands on remote surgery, diagnosis and so on. For example, in the diagnosis, the size of the tumor is an important factor to decide the stage of cancer. There are several techniques for 3D endoscopic systems, such as binocular stereo, active stereo by projector-camera pair, time of flight, etc. Among them, active stereo is one of the most promising techniques because of its simple configuration, *e.g.*, conventional endoscopic systems can be used without any modification. Although there are several issues to apply active stereo for endoscopic systems, such as dark and shallow focal range of the pattern projector, strong diffusion by tissue, etc., those issues are efficiently solved by a laser pattern projector recently [1, 2]. Those systems

use a micro-sized pattern projector with diffractive optical element (DOE) and have successfully reconstructed *ex vivo* human tumor samples. However, if we use the system with *in vivo* environment, other fundamental issues will arise; one is insufficient dynamic range of captured image because of the limited size of image sensor under no external light and the other is an unstable calibration of the system because of dynamic motion during an actual endoscopic operation.

In this paper, we proposed a new high dynamic range (HDR) imaging technique for a laser pattern projector as well an auto-calibration technique for dynamic motion. Usually HDR images are synthesized by using multiple-exposure images, however, it is usually impossible to precisely control the exposure of the camera of commonly available endoscopic systems. Therefore, we adopt to vary the intensity of the projector during the operation. In addition, to avoid complicated systems, we use simple signal switching (on-and-off) device without any synchronization mechanism. Multiple exposure images are efficiently captured by frequency difference between the camera and projector's fps. We also propose an auto-calibration technique realized by simultaneous capture of the head of the pattern projector as well as the projected pattern onto the target object. By softly imposing the 2-DOF ambiguity constraint [1], not only 6-DOF extrinsic parameters are robustly estimated, but also scale ambiguity is effectively eliminated.

By using our HDR synthesis technique and auto calibration algorithm, we can achieve an efficient and accurate reconstruction of tissue in metric 3D under practical operation of endoscopic system. In the experiments, we show the effectiveness of our technique with several tests using the real system, and demonstrate the successful reconstruction of the inside of real stomach of pig.

2 Related Work

3D endoscopes based on binocular stereo [3,4] are actively being researched at the present. For the binocular stereo algorithm, which is a typical passive stereo technique, correspondence retrieval is essentially difficult, especially on textureless surfaces. To cope with textureless surfaces, techniques using Shape from Shading (SfS) [5] have been proposed, however, the 3D reconstruction is only up-to-scale and it cannot be directly applied for measuring real sizes of 3D tissues. For laparoscopes for surgery, several structured-light systems have been already proposed [6,7].

An active stereo technique is a simple solution for the aforementioned problems. For example, a single-line laser scanner attached to the scope head was used to measure tissue shape [8]. However, the scope head had to be actuated in a direction parallel to the target, which limited the practical applicability of the technique. Some other vision techniques using special cameras being applied to endoscopes such as ToF sensors [9,10]. However, original resolution of ToF sensor is considerably low [9] or the size is too large and only applicable to laparoscope systems [10]. Recently, we proposed a structured light system for endoscope [1,2,11], which allows users to update a common endoscope system

without any reconfiguration. However, there are several problems with the system and our technique can provide practical solution.

One contribution of our technique is HDR image synthesis for endoscopic system. Usually HDR images are synthesized by using multiple-exposure images [12]. However, it is usually difficult to capture images with different exposures using ordinary video cameras. There are several techniques which achieve HDR synthesis and tone-mapping for video [13, 14], however active lighting conditions are not considered. If a lighting condition can be precisely controlled with camera synchronization, multi-exposure images are easily retrieved. Though, we assume only on-and-off controllable pattern projector with no synchronization mechanism, and there is no paper has published yet of such an approach.

In terms of auto-calibration, tons of techniques are proposed for binocular stereo so far [15]. However, there is a few techniques for active stereo systems, especially for structured light systems [16, 17]. It should be noted that scale ambiguity remains for common auto-calibration techniques and should be solved for endoscopic systems.

3 DOE-Based Laser Pattern Projector for Endoscopy

3.1 System Configuration

A projector-camera system is constructed by installing a micro pattern projector on a standard endoscope as shown in Fig. 1(a). For our system, we used a FujiFilm VP-4450HD system coupled with a EG-590WR scope. The DOE-based laser pattern projector is inserted in the endoscope through the instrument channel, the projector protrudes slightly from the endoscope head and emits structured light. The light source of the projector is a green laser module with a wavelength of 517 nm. The laser light is transmitted through a single-mode optical fiber to the head of the DOE projector. The DOE generates the pattern through diffraction of the laser light. The 3D measurements are conducted by structured light method with the projector-camera pair composed of the single endoscope camera and the pattern projector.

Our system is based on active stereo method that we have proposed [2], in which a gap-based grid pattern is used for avoiding effect of subsurface scattering that is harmful for 3D reconstruction. The projected pattern consists of only line segments as shown in Fig. 1(c) (top). The vertical lines of pattern are all connected and straight, whereas the horizontal segments are designed in a way to leave a small variable vertical gap between adjacent horizontal segments and their intersections with the same vertical line. With this configuration, a higher-level ternary code emerges from the design with the following three codewords: S (the end-points of both sides have the same height), L (the end-point of the left side is higher), and R (the end-point of the right side is higher). The codes of the pattern of Fig. 1(c) (top) are shown by color in Fig. 1(c) (bottom).

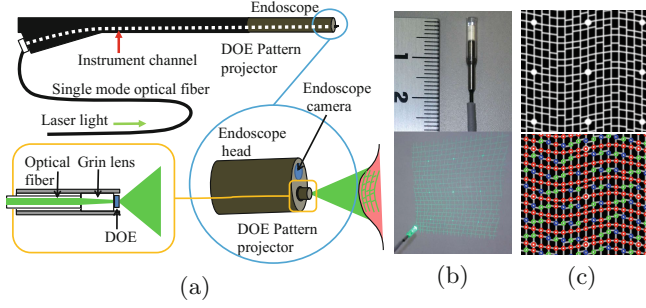


Fig. 1. System configuration: (a) System components. (b) DOE micro projector. (c) The projected pattern(top), and embedded codewords of S colored in red, L in blue, and R in green (bottom). S means edges of the left and the right sides have the same height, L means the left side is higher, and R means the right is higher. (Color figure online)

3.2 3D Reconstruction

The source image is first geometrically corrected on the fish-eye lens distortion. Noises of the image are suppressed using Gaussian filters or median filters at the same time. The projected vertical and horizontal lines are detected in the undistorted image using the line detection algorithm from Sagawa *et al.* [18]. This method can detect projected parallel lines whose approximate directions are known, ignoring intersecting non-vertical lines, based on loopy belief propagation.

From the detected line patterns, grid-graph structure is constructed by detecting intersections between the horizontal and vertical lines. Then, each node is connected with its up, down, left, or right adjacent nodes by vertical or horizontal edges. Some horizontal edges might have a missing edge because of misdetection. In this case, the node will only have either a left or a right edge, which may be later matched by looking at other connectivity of the grid graph. Figures 8(f) and 9(b)(f) show examples of the detected vertical and horizontal patterns with estimated gap codes.

Let the detected grid-graph be G , and let the grid-graph of the pattern in Fig. 1(c) be P . Note that graph G may lack some edges, or have undesired false edges, missing labels, or false labels of $S/L/R$ as shown in the left part of Fig. 2.

To match G and P allowing topological errors, we exploit the notion of local sub-graph patterns (LSGPs). We define an LSGP to be a sub-graph of a grid-graph used as a template for matching common local topologies of G and P (in Fig. 2, the left part shows G , the right part shows P , and the middle part shows LSGPs). Given a dictionary of LSGPs, G may be matched to P robustly to missing or false edges. By providing multiple LSGPs and trying to match G and P using each of them, flexible matching can be realized. In our implementation, an LSGP is represented by a path that traces all of its edges. To merge all the matching results of LSGPs, voting is used.

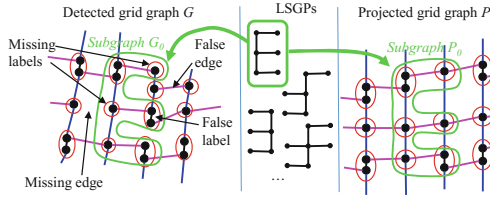


Fig. 2. Matching the detected grid graph and the projected pattern using LSGPs.

Once the correspondence of the captured image to the pattern is obtained, the points on the vertical and horizontal lines are reconstructed in 3D using a light-sectioning method.

4 Auto-Calibration of the Projector Position

In this system, the target surface, which is projected by pattern projector, is captured by the endoscope camera. Since the head of the projector is not tightly fixed to the endoscope, the relative position between the projector head and the endoscopic camera varies during endoscopic operations, such as bending the head. Since, for active stereo techniques, the position of the projector is an important parameter for 3D reconstruction, such unstable condition is problematic for robust and accurate shape measurement.

Furukawa *et al.* [1] modeled the relative position by 2-DOF rigid transformation, where projector translates along or rotates around the axis of the instrument channel. This 2-DOF model could be applied to our system if the pattern projector’s outer diameter perfectly fitted to the inner diameter of the instrument channel. However, there should be some margin between the projector and the channel, for the projector to be inserted during the endoscopic operations. In real situations, the projector have more freedom to move beyond the 2-DOF model within the margin.

Another problem of work of Furukawa *et al.* [1] is that they estimate the projector’s position by detecting a marker drawn on the projector from the endoscope image. In real situations where endoscope image is captured in dark environments, markers drawn on the projector are difficult to detect from the captured images.

In the proposed system, we use silhouette of the projector and the markers embedded in the grid pattern projected onto the target surface. The silhouette of the projector can be observed from the captured image, even if there are not illumination except for the projected pattern. The markers in the grid pattern can be also detected from the same image (see Fig. 8(d) for an example, where the projector silhouette can be observed at the bottom of the image).

The actual process is as follows: From the input image captured for measurement, markers in the grid patterns (m_i) are detected. Also, several points in the projector’s silhouette (s_j) are also sampled (Fig. 3). Note that, we can

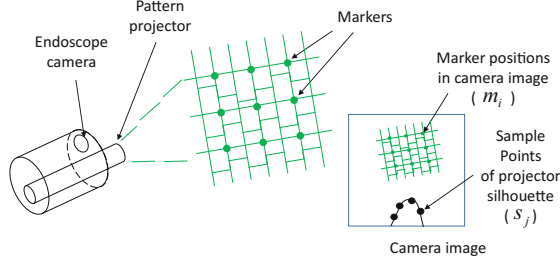


Fig. 3. Input points for auto-calibration of the projector.

assume epipolar geometries fulfilled between the endoscope camera and the pattern projector, if the estimated parameters are correct for the auto-calibration. Since a pattern projector can be modeled in the same way as a camera, epipolar geometries can be used for a projector-camera pair.

The auto-calibration is processed as an optimization of 6-DOF rigid transformation parameters that represent projector's position. Here, we divide the estimated 6 parameters into 2 sets of parameters: one set is for 2-DOF freedom described in [1] and the other is for the rest 4 parameters. We regard the 2-DOF parameters as freely changing parameters, since they represent the motion of the pattern projector that rotates around and translates along the axis of the instrument channel, while we suppress the rest 4 parameters since they are deviation from the 2-DOF freedom of [1]. Because of this 'soft' 2-DOF constraint, the estimated projector position does not have scale ambiguity.

The optimized cost function is defined as follows:

1. The cost function takes 6 parameters $p_1, p_2, q_1, q_2, q_3, q_4$, representing the 3D position of the projector (rotation \mathbf{R} and translation \mathbf{t}) relative to the endoscope camera, where p_1 and p_2 are 2-DOF parameters described in [1], and q_1, \dots, q_4 represents the rest of the full 6-DOF rigid transformation that should be suppressed.
2. For the markers m_i , the corresponding epipolar line is calculated, and the distance between m_i and the epipolar line is calculated as g_i .
3. The virtual silhouette of the projector is rendered as a cylinder moved by the rigid transformation \mathbf{R} and \mathbf{t} . From each s_j , the minimum distance from s_j to contours of the rendered silhouette is calculated as h_j .
4. $\sum_i (g_i)^2 + w_1 \sum_j (h_j)^2 + w_2 \sum_k (q_k)^2$ is calculated as the cost value, where w_1 is weight of the cost of silhouette fitting and w_2 is weight for suppression of the parameters representing the deviation from the 2-DOF freedom [1].

In current implementation, selection of the marker position and sampling points on the silhouette contour are conducted manually for each frame in image sequences and auto-calibration should be conducted for each frame. Further automation for point selection will be our future work.

5 HDR Synthesis Using Asynchronous Blinking Pattern

To synthesize HDR image, usually multiple-exposure images are required. However, it is not possible to capture such images with commonly available endoscopic systems. To solve the issue, we control the light source instead of the camera, *i.e.*, blinking the pattern in this paper. Note that we just switch the pattern on-and-off periodically without synchronization mechanism, such an implementation is simple and easy.

The reason why just two intensities for the projector are fine to synthesize HDR whereas usually multiple exposures are required, is based on the difference of frequency of the camera and the projector. Suppose n Hz for the camera and m Hz for the projector. Usually video mode of camera is set burst mode, *i.e.*, the shutter is always open, and the shutter speed is $1/n$ sec. On the other hand, switching (on-and-off) signal makes half of exposure time, *i.e.*, $1/(2m)$ for the projector. Then the exposure time is $1/(2m) - s$, when the offset is s ($s < 1/(2m)$, $n < 2m$). Since s varies at each capture because of the frequency difference, exposure time is also changed at each capture as shown in Fig. 4. For example, if $n = 30$ and $m = 26$, then exposure time varies approximately with 8 Hz and we can synthesize HDR using the 8 frames. Then, tone mapping is applied to the HDR images to make 8bit images, which allows to use conventional image processing tools.

To make HDR, exposure time is supposed to be known. If the camera and the projector are synchronized, the s is known and an exact exposure time can be calculated. However, it requires a complicated device to achieve synchronization. To avoid such additional devices, we estimate the exposure time only from captured images. In our implementation, we simply average the intensity of the pattern excluding outliers with simple thresholding technique for each frame and use the ratio of the average as for the ratio of exposure time.

Normally, multiple-exposure for HDR image synthesis is conducted for a static camera and the scene. Since the endoscope and the target tissue can be move, they are not static. However, for the above setup of $n = 30$ and $m = 26$, we can obtain a image set of around 8 different exposure in $1/4$ s, which is short enough to assume the camera and the scene is static if we hold the endoscope still.

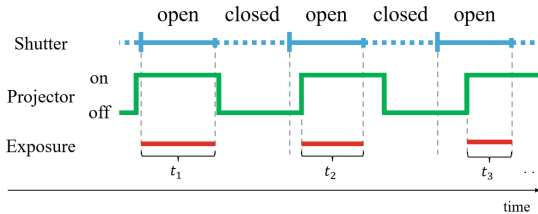


Fig. 4. Relationship between a shutter speed and a pattern projection time: t_i represents an exposure time.

6 Experiments

6.1 Improvement Using HDR Image for 3D Reconstruction

To show effectiveness of the HDR image generation, we tested our algorithm using a human hand as the target object. We first captured images of the target surface which is projected by a blinking laser pattern projector. Although pattern is just illuminated bright and dark repeatedly, we could obtain an image sequence with different exposures. We have extracted 8 images of one multi-exposure cycle I_1, I_2, \dots, I_8 . I_1, I_3, I_5 and I_7 are shown in Fig. 5. With our HDR image synthesis method, image sequence of single period of intensity change is automatically extracted by finding the darkest frame in three consecutive frames; Fig. 5 is one of such sequence.

Then, HDR image is created from the sequence, and then, tone-mapped for 3D reconstructed algorithm. The HDR image is shown in Fig. 6(b). The 3D reconstructed results with/without HDR algorithm are shown in Fig. 6(c) and (d). The numbers of reconstructed points for each frame and HDR image are shown in Fig. 7. From Fig. 7, we can confirm that the area that was successfully reconstructed from the HDR image was larger than the results of the any of the original input images. In Fig. 6, we can see that the regions around the brightest center marker were reconstructed in the result of I_T (HDR image), whereas, in

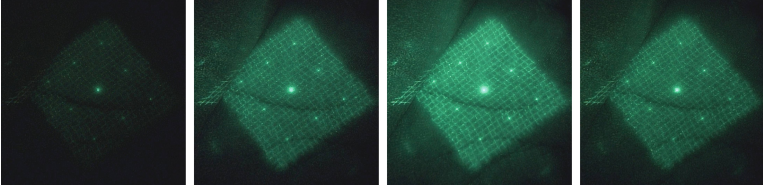


Fig. 5. Original images: I_1, I_3, I_5, I_7 from 8 images I_1, I_2, \dots, I_8 . Note that the exposure was changing frame by frame.

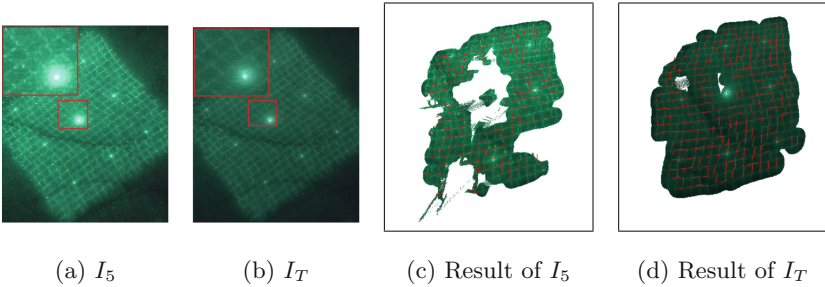


Fig. 6. Comparison between the original and the tone-mapped HDR images. (a) I_5 from Fig. 5, which was most successfully reconstructed in images I_1 to I_8 . (b) The tone-mapped HDR image generated from I_1 to I_8 . (c) 3D reconstruction result of (a). (d) 3D reconstruction result of (b).

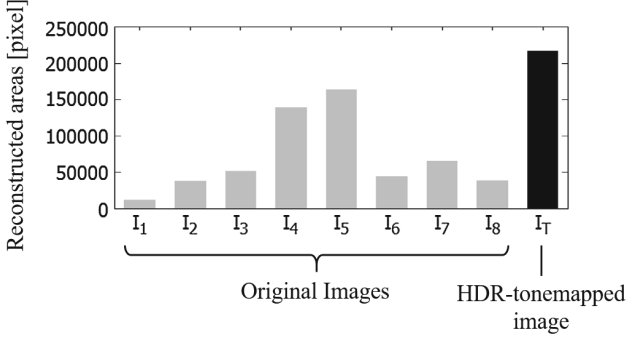


Fig. 7. Comparison of 3D reconstructed areas of original and tone-mapped HDR images.

the result of I_5 (note that I_5 was the most successfully reconstructed image from Fig. 7), the same regions were not reconstructed. In Fig. 6, we can also see that the noises in the source images are reduced in the tone-mapped HDR image, because multiple images are merged so that independent noises are suppressed. From the results, we have confirmed that HDR image enhanced the image quality and reduced the negative effects of over and under exposures and noises.

6.2 3D Reconstruction Inside Stomach of a Pig

To evaluate the system in more realistic conditions, we captured shapes inside a stomach of a pig, which is often used for evaluation purpose and practice of endoscopists. To evaluate the scales captured by the 3D endoscope, we first curved several markers on the surface of pig’s stomach, then, reconstruct 3D shape of the entire surface. The distances between the two markers are estimated and compared to the ground truth, which is obtained by measuring the real distances between the markers after the measurement process; we cut and opened the stomach. Since the stomach was inflated while the endoscopy diagnosis, the ground truth distances that are actually measured were considered to be smaller than the estimated distance with our technique. To compensate such error, we also measure the ground truth distance while expanding the stomach surface manually.

Figure 8 shows the experimental situation and the measurement results. Comparison between estimated results and ground truth are shown in Table 1. The precision was about 5.0% and 2.1% from the unexpanded ground truth. Considering the difference of measurement situation, we could conclude that the measurement was sufficiently accurate. In Fig. 8(g) and (h), we also show the result of auto-calibration. In Fig. 8(g), which shows situation before auto-calibration, the rendered silhouette of the projector is different from the captured silhouette of Fig. 8(e). After auto-calibration shown in Fig. 8(h), the projector position fits to the captured image, and the epipolar lines lie on the marker position.

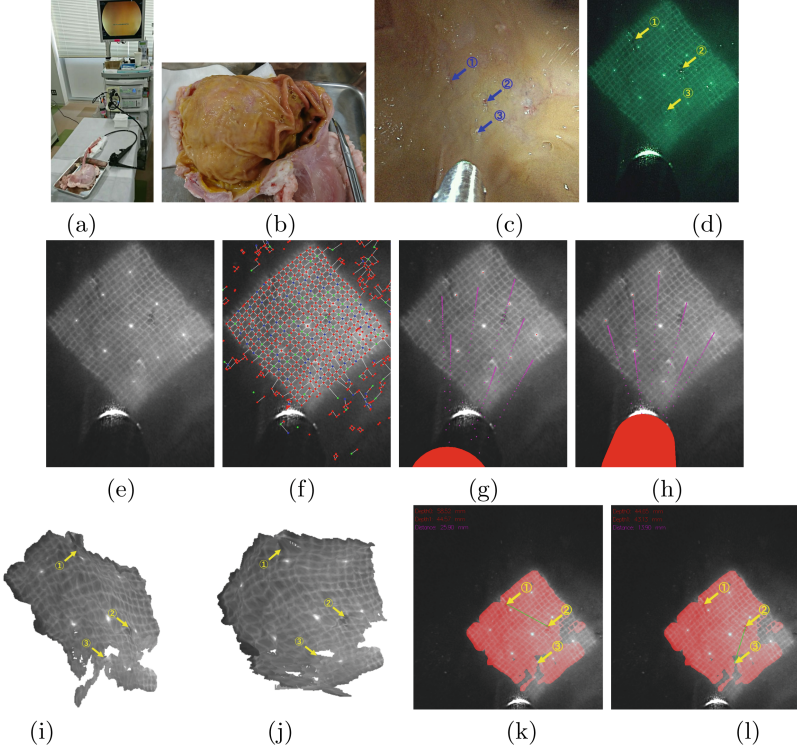


Fig. 8. 3D reconstruction of bio-tissue inside a pig stomach with markers. (a) The environment of the experiment. (b) The pig-stomach cut open after experiment session. (c) The appearance inside the stomach with marker positions. (d) The captured image with the pattern projected. (e) The HDR enhanced image. (f) The detected grid graph. (g), (h) Before and after the auto-calibration of the projector. The rendered projector posing is the read cylinder and the epipolar lines are pink line segments. (g) is before the auto-calibration and (h) is after the auto-calibration. (i), (j) Reconstructed 3D shape rendered from two different view points. (k), (l) Distance measurements between the two markers. Red regions are reconstructed areas. (Color figure online)

Table 1. Estimated distances between two markers of pig stomach

Marker IDs	Ground Truth	Ground Truth (expanded)	Our result
1 and 2	24.6 mm	29.4 mm	25.9 mm
2 and 3	14.2 mm	15.1 mm	13.9 mm

While measuring the pig’s stomach, we also measured more complicated shapes such as ridges on the surface. Figure 9 shows examples of the captured images and the reconstructed shapes. We can confirm that the ridges or concaves

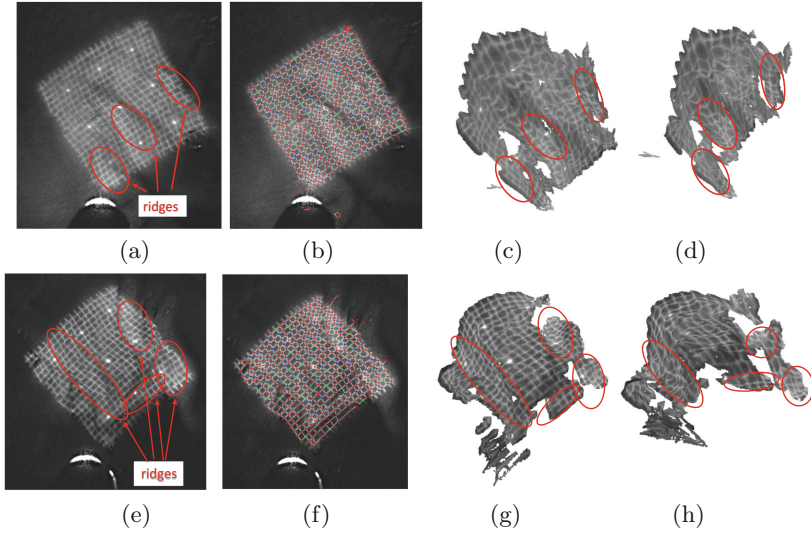


Fig. 9. 3D reconstruction of bio-tissue inside a stomach with complicated shapes. (a) The HDR processed input image. (b) The detected grid graph with codes. (c)(d) The reconstructed shapes viewed from different directions. (e)–(h) Another result. Note that ridges of the surface are successfully reconstructed in the 3D shape.

of the bio-tissues are captured in the 3D reconstruction results, which proves that our technique can recover dense shape of complicated surfaces.

7 Conclusion

We proposed a 3D endoscopic system based on an active stereo, where the laser pattern projector consists of a DOE that generates a special line-based grid pattern. Since the laser projector has a strong light intensity and dynamic range of the camera is not enough, we propose a new HDR image synthesis technique using a blinking modulation applied to the projector. In addition, the head of endoscope dynamically moves during an actual operation, and thus, the relative position of a camera and a projector is not fixed with respect to each other. Since the relative position should be known for 3D reconstruction, we propose an auto-calibration technique using the silhouette of the pattern projector. The ability of the techniques were confirmed by intensive experiments using real endoscopic systems and demonstrated by reconstructing the 3D shape of the inside surface of a pig’s stomach. Our future work is to construct the realtime system and use it to actual diagnosis and operations.

References

1. Furukawa, R., Masutani, R., Miyazaki, D., Baba, M., Hiura, S., Visentini-Scarzanella, M., Morinaga, H., Kawasaki, H., Sagawa, R.: 2-dof auto-calibration for a 3D endoscope system based on active stereo. In: 2015 37th Annual International Conference of the IEEE Engineering in Medicine and Biology Society (EMBC), pp. 7937–7941, August 2015
2. Furukawa, R., Sanomura, Y., Tanaka, S., Yoshida, S., Sagawa, R., Visentini-Scarzanella, M., Kawasaki, H.: 3D endoscope system using doe projector. In: The 38th Annual International Conference of the IEEE Engineering in Medicine and Biology Society (EMBC 2016) (2016)
3. Nagakura, T., Michida, T., Hirao, M., Kawahara, K., Yamada, K.: The study of three-dimensional measurement from an endoscopic images with stereo matching method. In: Automation Congress, 2006. WAC 2006. World, pp. 1–4, July 2006
4. Stoyanov, D., Scarzanella, M.V., Pratt, P., Yang, G.-Z.: Real-time stereo reconstruction in robotically assisted minimally invasive surgery. In: Jiang, T., Navab, N., Pluim, J.P.W., Viergever, M.A. (eds.) MICCAI 2010. LNCS, vol. 6361, pp. 275–282. Springer, Heidelberg (2010). doi:[10.1007/978-3-642-15705-9_34](https://doi.org/10.1007/978-3-642-15705-9_34)
5. Visentini-Scarzanella, M., Stoyanov, D., Yang, G.: Metric depth recovery from monocular images using shape-from-shading and specularities. In: ICIP, Orlando, USA, pp. 25–28 (2012)
6. Maurice, X., Albitar, C., doignon, C., de Mathelin, M.: A structured light-based laparoscope with real-time organs' surface reconstruction for minimally invasive surgery. In: 2012 Annual International Conference of the IEEE Engineering in Medicine and Biology Society, pp. 5769–5772, August 2012
7. Reiter, A., Sigaras, A., Fowler, D., Allen, P.K.: Surgical structured light for 3D minimally invasive surgical imaging. In: 2014 IEEE/RSJ International Conference on Intelligent Robots and Systems, pp. 1282–1287, September 2014
8. Grasa, O., Bernal, E., Casado, S., Gil, I., Montiel, J.: Visual slam for handheld monocular endoscope. *IEEE Trans. Med. Imaging* **33**(1), 135–146 (2014)
9. Köhler, T., Haase, S., Bauer, S., Wasza, J., Kilgus, T., Maier-Hein, L., Feußner, H., Hornegger, J.: ToF meets RGB: novel multi-sensor super-resolution for hybrid 3-D endoscopy. In: Mori, K., Sakuma, I., Sato, Y., Barillot, C., Navab, N. (eds.) MICCAI 2013. LNCS, vol. 8149, pp. 139–146. Springer, Heidelberg (2013). doi:[10.1007/978-3-642-40811-3_18](https://doi.org/10.1007/978-3-642-40811-3_18)
10. Penne, J., Schaller, C., Engelbrecht, R., Maier-Hein, L., Schmauss, B., Meinzer, H.P., Hornegger, J.: Laparoscopic quantitative 3D endoscopy for image guided surgery. In: Bildverarbeitung für die Medizin, Citeseer, pp. 16–20 (2010)
11. Furukawa, R., Aoyama, M., Hiura, S., Aoki, H., Kominami, Y., Sanomura, Y., Yoshida, S., Tanaka, S., Sagawa, R., Kawasaki, H.: Calibration of a 3d endoscopic system based on active stereo method for shape measurement of biological tissues and specimen. In: EMBC, pp. 4991–4994 (2014)
12. Debevec, P.E., Malik, J.: Recovering high dynamic range radiance maps from photographs. In: SIGGRAPH 2008, pp. 1–10. ACM, New York (2008)
13. Kalantari, N.K., Shechtman, E., Barnes, C., Darabi, S., Goldman, D.B., Sen, P.: Patch-based high dynamic range video. *ACM Trans. Graph.* **32**(6), 202–1 (2013)
14. Eilertsen, G., Mantiuk, R., Unger, J.: A comparative review of tone-mapping algorithms for high dynamic range video. In: Computer Graphics Forum, vol. 36, pp. 565–592. Wiley Online Library (2017)

15. Forsyth, D., Ponce, J.: Computer Vision: A Modern Approach, 2nd edn. Pearson Education Inc., London (2011)
16. Furukawa, R., Kawasaki, H.: Laser range scanner based on self-calibration techniques using coplanarities and metric constraints. *Comput. Vis. Image Underst.* **113**(11), 1118–1129 (2009)
17. Furukawa, R., Kawasaki, H.: Self-calibration of multiple laser planes for 3D scene reconstruction. In: 3DPVT, pp. 200–207 (2006)
18. Sagawa, R., Ota, Y., Yagi, Y., Furukawa, R., Asada, N., Kawasaki, H.: Dense 3D reconstruction method using a single pattern for fast moving object. In: ICCV (2009)

Computer Assisted and Robotic Endoscopy and Clinical
Image-Based Procedures

4th International Workshop, CARE 2017, and 6th
International Workshop, CLIP 2017, Held in Conjunction
with MICCAI 2017, Québec City, QC, Canada, September
14, 2017, Proceedings

Cardoso, J.; Arbel, T.; Luo, X.; Wesarg, S.; Reichl, T.;
González Ballester, M.Á.; McLeod, J.; Drechsler, K.;
Peters, T.M.; Erdt, M.; Mori, K.; Linguraru, M.G.; Uhl, A.;
Oyarzun Laura, C.; Shekhar, R. (Eds.)

2017, XIV, 182 p. 86 illus., Softcover

ISBN: 978-3-319-67542-8